Multidisciplinary Journal of Engineering and Technology

Print ISSN: 3007-6897 Online ISSN: 3007-6900

DOI: https://doi.org/10.61784/mjet3031

ENERGY AND MAGNETIC FIELD DISTRIBUTION CHARACTERISTICS OF PM AND JONSWAP SPECTRA

XinTong Wang*, JianSheng Zhang

Department of Physics, School of Sciences, Xi'an Technological University, Xi'an 710021, Shaanxi, China.

Corresponding Author: XinTong Wang, Email: 1820510675@qq.com

Abstract: To further investigate the formation mechanism, distribution characteristics, and distribution patterns of wave-induced magnetic fields, this study employs the Pierson-Moskowitz wave spectrum combined with the JONSWAP spectrum and Weaver electromagnetic theory. Using Monte Carlo random sampling, it simulates the dynamic characteristics of a two-dimensional sea surface under varying wind speeds. Maxwell's equations are applied to formulate expressions for the wave-induced magnetic field. The primary focus is simulating the three-dimensional spatial distribution and spectral characteristics of the induced magnetic field under different wind speed scenarios. Simulation results indicate: The PM spectrum is suitable for describing fully developed sea conditions characterized by uniform wave energy distribution and gentle waveforms. The JONSWAP spectrum is more applicable to developing wind-driven waves, exhibiting concentrated energy, steep waveforms, and higher induced magnetic field intensities. As wind speed increases, both spectra exhibit a trend of peak frequency migration toward lower frequencies. The induced magnetic field amplitude corresponding to the JONSWAP spectrum is significantly higher than that of the PM spectrum. These findings provide theoretical and simulation support for noise modeling and signal extraction in marine electromagnetic detection.

Keywords: Pierson-Moskowitz wave spectrum; JONSWAP spectrum; Wave-induced magnetic field

1 INTRODUCTION

In the early 1960s, Pierson and Moskowitz [1] derived the Pierson-Moskowitz (P-M) wave spectrum from measured data in the North Atlantic, based on the Neumann spectrum. This spectrum was established using spectral estimation combined with curve fitting, derived from measured results of fully developed wind waves. Between 1968 and 1969, the Joint North Sea Wave Project (JONSWAP) was conducted by relevant institutions from the UK, Netherlands, USA, Germany, and other countries. Systematic wave observations were conducted from the west coast of the island of Sylt, located at the border between Denmark and Germany, in a west-northwest direction. Based on these field measurements, the JONSWAP spectrum was proposed between 1971 and 1973.

Scholars have long conducted in-depth research on wave spectra. Weaver [2] was the first to incorporate magnetic induction effects into his study, deriving the magnetic field of surface waves using differential expressions of Faraday's and Ampere's laws. Pedersen et al.[3] investigated the correlation between wave surges and magnetic field signals. Through comprehensive analysis of data collected in the Southern Ocean, they characterized these properties, providing a reference for aeromagnetic surveys. Tang Jinfeng et al.[4] derived wave distribution parameters based on actual measurements of wave height and period in China's coastal waters, enabling numerical simulation of wave processes to obtain the induced magnetic field spectrum under real sea conditions. Zhang Zili et al. [5] conducted a detailed study on the spectral characteristics of the induced magnetic field from two-dimensional infinite-depth ocean waves. Zhu Xiaojian et al. [6] analyzed the magnetic field response of multi-frequency ocean waves in a three-dimensional infinitedepth environment through frequency superposition processing of the wave-induced magnetic field. Wang Wei [7] derived an evaluation method for ship wake magnetic fields under wind-wave conditions, employing mathematical models to describe the induced magnetic field characteristics of wind-wave wakes and deriving the correlation between wind speed and magnetic fields. Zhang Baoqiang [8] established a three-dimensional finite-depth single-frequency wave-induced electromagnetic field model using the direct differentiation method. Lin Zhiheng et al. [9] calculated twodimensional wave-induced magnetic fields using Biot-Savart's law. Zhou Chun et al. [10] solved wave-induced magnetic fields based on the Green's function method. Zhang Jiansheng [11] pioneered systematic measurements of wake optical properties, establishing a core theoretical framework for underwater optical detection. Through numerical simulation analysis, Zhang Chengji [12] and Xiao Chen [13] respectively obtained the distribution patterns of ship wake-induced magnetic fields and the electromagnetic characteristics of bubble curtains. Yan Linbo et al. [14] achieved computer simulations of magnetic field anomalies in multi-ship wakes, completing characteristic analyses across multidimensional scenarios. For KCS standard ship models, Lan Qing et al. [15] performed detailed simulation analysis of wake-induced electromagnetic fields. As a highly conductive medium, seawater moving within the geomagnetic field generates induced electromagnetic fields, with wave-induced magnetic fields being the most pronounced. These fields constitute a critical noise source affecting marine electromagnetic data quality. Researchers worldwide have conducted a series of explorations into wave-induced magnetic phenomena, gradually developing relevant theoretical models and numerical solutions. Weaver established a magnetic response model for wave-geomagnetic interactions using Maxwell's equations, providing a theoretical framework for subsequent research. Previous studies primarily focused on

theoretical modeling under idealized conditions, with limited systematic simulation and analysis of the spatial and spectral characteristics of wave-induced magnetic fields under real sea conditions caused by varying wind speeds. Building upon Weaver's electromagnetic theory, this study compares the energy characteristics of PM and JONSWAP spectra with those of wave-induced magnetic fields. Employing the Monte Carlo method to simulate random sea surfaces under varying wind speeds, it combines Maxwell's equations with derivation processes to derive analytical expressions for induced magnetic fields. with a focus on investigating the spatial distribution and spectral characteristics of the wave-induced magnetic field. This provides theoretical support and simulation data for noise modeling and signal extraction in marine electromagnetic detection.

2 THEORETICAL BASIS

2.1 PM Spectrum

The P-M spectrum originates from Pierson and Moskowitz's (1964) statistical analysis of fixed-point observation data in the North Atlantic. It applies to open ocean areas without restricted wind zones, specifically fully developed waves. The mathematical form of the P-M spectrum can be written as:

$$S(\omega) = \frac{\alpha g^2}{\omega^5} \exp\left[-\beta \left(\frac{g}{\omega U}\right)^4\right]$$
 (1)

In the equation, the dimensionless constant $\alpha = 8.10 \times 10^{-3}$, $\beta = 0.74$; U represents the wind speed at a height of 19.5 meters above sea level. Although the P-M spectrum falls under the category of empirical spectra, its empirical results are relatively reliable. Its structure is straightforward, requiring fewer parameters, making it easy to grasp and highly practical. Its applications span multiple fields including wave analysis, marine development, coastal engineering, and ship engineering, yielding significant results.

2.2 JONSWAP Spectrum

In the late 1960s, relevant agencies from the United Kingdom, the Netherlands, the United States, Germany, and other countries proposed the JONSWAP spectrum during the Joint North Sea Wave Project (JONSWAP). This spectrum is applicable to sea areas with restricted wind ranges. The spectral formula for this spectrum is:

$$S(\omega) = \frac{\alpha g^2}{\omega^2} \exp\left[-1.25 \left(\frac{\omega_p}{\omega}\right)^4\right] \gamma^{\exp\left[\frac{-(\omega - \omega_p)^2}{2\sigma^2 \omega_p^2}\right]}$$
(2)

In the formula $\alpha = 0.0067 \left(gx/U^2\right)^{-0.22}$, where x is the wind distance (m) and U is the average wind speed (m/s); ω_p is the spectral peak frequency (s^{-1}) , typically set to $\omega_p = 22 \left(g/U\right) \left(gx/U^2\right)^{-0.33}$; γ is the spectral peak enhancement factor, $\gamma = E_{\text{max}} / E_{\text{max}}^{PM}$, E_{max} where and E_{max}^{PM} represent the spectral peak value and the peak value of the P-M spectrum, respectively. The range of is 1.5 to 6.0, with the average value of 3.3 commonly used; σ is the peak shape parameter. When $\omega \leq \omega_p$, σ is set to 0.07; when $\omega \geq \omega_p$, σ is set to 0.09.

2.3 Theory of Wave-Induced Magnetic Fields

The electric field strength induced by ocean waves in the Earth's magnetic field Magnetic flux density satisfies Maxwell's equations of electromagnetic theory:

$$\nabla \times \mathbf{E} = -\partial \mathbf{B} / \partial t \tag{3}$$

$$\nabla \times \mathbf{B} = \mu \mathbf{J} + \mu \varepsilon (\partial \mathbf{E} / \partial t) \tag{4}$$

In the equation, μ is the magnetic permeability in vacuum, with a value of $4\pi \times 10^{-7}$; \mathcal{E} is the dielectric constant of seawater; J is the conductive current density. The conductive current density in seawater consists of two components: ∂E where $\sigma(V \times F)$ is the velocity of V seawater motion, F is the geomagnetic field strength, and σ is the electrical conductivity of seawater. In seawater, the electrical conductivity is equal to 4S/m, and the dielectric constant is equal to $7.08 \times 10^{-4} \, F/m$. Therefore, the conductive current is much greater than the displacement current. The second term on the right-hand side of equation (3) can be neglected.

The mathematical model of wave motion generated by Weaver in the geomagnetic field is shown in Figure 1. In the figure, Oxyz is a Cartesian coordinate system. The axis z points toward the seafloor (positive direction), and the axis x points in the direction of wave propagation (z = 0), The origin lies at the sea surface. a represents the amplitude of the wave motion. I denotes the magnetic inclination angle, and θ denotes the angle between the horizontal direction of the

ocean current and the geographic North Pole. The unit vectors of the and axes are denoted by i, j, k and x, y, z, respectively.

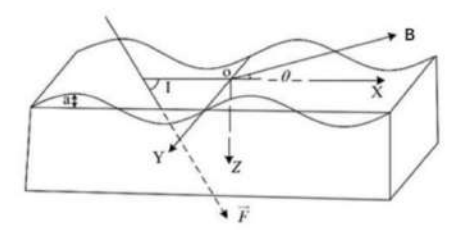


Figure 1 Mathematical Model of Weaver

Assuming the magnitude of the magnetic field's magnetic induction is constant, it follows from Figure 1 that

$$F = F(\cos I \cos \theta \mathbf{i} - \cos I \sin \theta \mathbf{j} + \sin I \mathbf{k})$$
(5)

Equation (3) indicates that the first step in solving for the induced magnetic field is to calculate B. To this end, the velocity potential function is introduced φ . By performing a gradient calculation on the velocity potential function, the following can be obtained V:

$$V = \nabla \phi \tag{6}$$

Sea waves can be modeled as plane harmonic waves with angular frequency ω , thus varying over time in the form $e^{i\omega t}$. For a free-surface sea, the amplitude of a wave motion is much smaller than the wavelength. Consequently, the x-direction solution for sea waves corresponding to equation (5) is given by:

$$\varphi = \frac{ag}{\omega} \exp(i\omega t - imx - mz) \tag{7}$$

In the equation, a is the amplitude $m = \omega^2 / g$, and (where is the g gravitational acceleration), so the velocity of the sea water motion is obtained [16].

$$V = -a\alpha(i\mathbf{j} + \mathbf{m})\exp(i\alpha t - in\mathbf{x} - n\mathbf{z})$$
(8)

a as frequency varies, $a = \sqrt{2S(\omega)}$ within a unit frequency interval, where is the $S(\omega)$ wave spectrum.

Since velocity is a sinusoidal function varying only with time and coordinate, it is evident that the electromagnetic field induced by the motion of seawater also takes a sinusoidal form. The magnitudes of the electric field intensity vector and magnetic flux density vector vary with depth, so they can be expressed as

$$B = b(z) \exp(i\omega t - imx)$$

$$E = e(z) \exp(i\omega t - imx)$$
(9)

In the equation, b is the amplitude vector of the magnetic field vector; e is the amplitude vector of the electric field vector. Taking the $b = b_x i + b_y j + b_z k$ divergence of both sides of equation (2) using yields:

$$\frac{db_z}{dz} = imb_x \tag{10}$$

Taking the curl of both sides of equation (3) and substituting equations (4) to (8) yields

$$\frac{\mathrm{d}^2 \boldsymbol{b}}{\mathrm{d}z^2} = (m^2 + \mathrm{i}\gamma)\boldsymbol{b} - A\gamma(\boldsymbol{i}\boldsymbol{j} + \boldsymbol{k})\exp(mz)$$
(11)

In the equation, $A = amF(\sin I + i\cos I\cos\theta)$, $\gamma = \mu\sigma\varepsilon$.

According to the uniqueness theorem for electromagnetic fields, the vertical component of magnetic flux density at the sea surface must be continuous. From this boundary condition, the vertical component of magnetic flux density generated by ocean waves can be solved as follows:

$$b_z = iA \left\{ \frac{2}{1 + (1 + i\beta)^{1/2}} \exp\left[-mz(1 + i\beta)^{1/2}\right] - \exp(-mz) \right\}$$
 (12)

In the equation, $\beta = \frac{\gamma}{m^2} = \frac{\mu \sigma g^2}{\omega^3}$, Substituting expression (11) into expression (9) yields the horizontal component of the magnetic flux density generated by the wave.

$$b_x = -A \left\{ \frac{2(1+i\beta)^{1/2}}{1+(1+i\beta)^{1/2}} \exp[-mz(1+i\beta)^{1/2}] \exp(-mz) \right\}$$
 (13)

The typical period of ocean wave fluctuations is mostly between 10 and 20 seconds[17]. For actual ocean surface waves, this β is a very small value, allowing equations (11) and (12) to be approximated as follows:

$$b_z = \frac{1}{4}\beta_A(2mz + 1)\exp(-mz)$$
 (14)

$$b_x = \frac{1}{4}i\beta_A(2mz+1)\exp(-mz)$$
 (15)

Using equation (8), the expressions for the components of the magnetic induction intensity induced by ocean waves are given by:

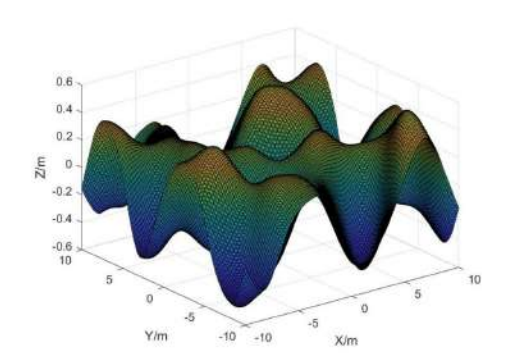
$$B_z = \frac{1}{4} \beta_A \left(2_{mz} + 1 \right) \times \exp(-mz) \exp\left[i(\omega t - mx + \frac{\pi}{2})\right]$$
 (16)

$$B_x = \frac{1}{4} \beta_A \left(2_{mz} + 1 \right) \times \exp(-mz) \exp[i(\omega t - mx)]$$
 (17)

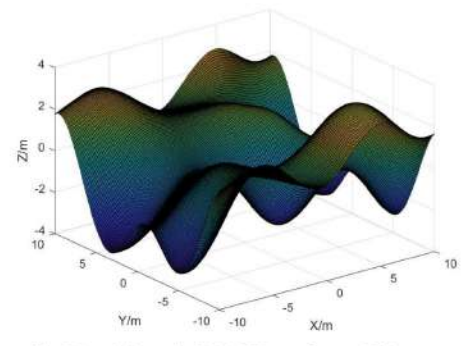
3 SIMULATION COMPUTING

3.1 PM Spectrum and JONSWAP Spectrum 3D Waveform Diagram

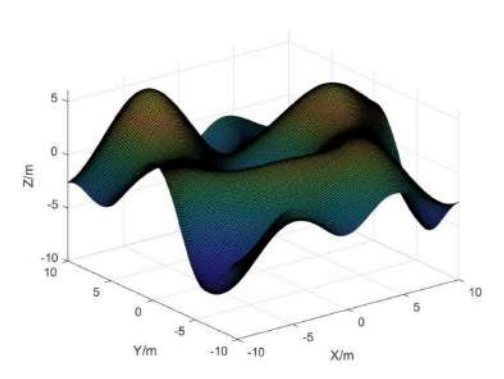
Based on the Pierson-Moskowitz (P-M) and JONSWAP wave spectra, a two-dimensional random sea surface was generated using the Monte Carlo method. The simulation parameters were set as follows: wave length $\lambda=0.3$ m, simulation area range in both X and Y directions set to [-10 m, 10 m], spatial sampling point interval of 1 m; Wave propagation occurs along the positive X-axis direction. Wind speeds of 5 m/s, 10 m/s, and 15 m/s were applied, with gravitational acceleration g=9.8 m/s². The simulation results are shown in the figure.



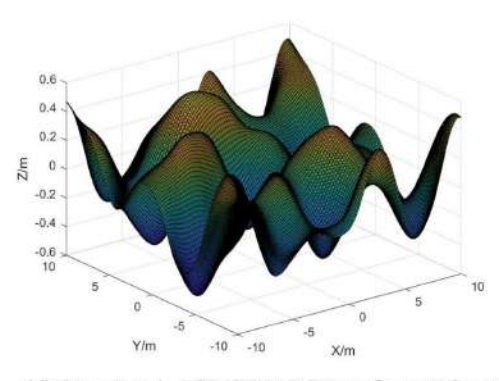
(a) V = 5 m/s PM Waveform Diagram



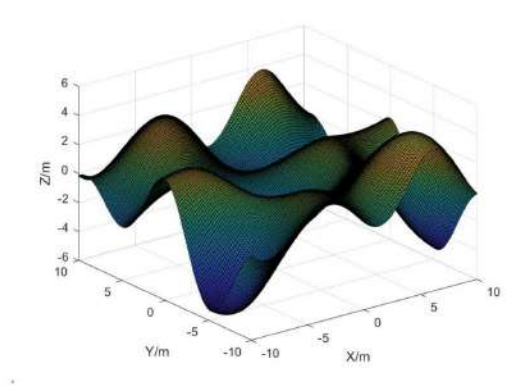
(b) V = 10 m/s PM Waveform Diagram

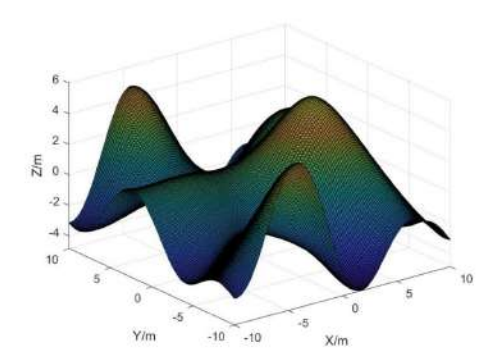


(c) V = 15 m/s PM Waveform Diagram



(d) V = 5 m/s JONSWAP Waveform Diagram





(e) V = 10 m/s JONSWAP Waveform Diagram (f) V = 15 m/s JONSWAP Waveform Diagram Figure 2 Three-Dimensional Waveform Diagram of Sea Waves

From Figures 2 (a), (b), and (c), the waveform characteristics of the PM spectrum at wind speeds of 5 m/s, 10 m/s, and 15 m/s can be observed. Analysis of the waveform morphology reveals that the PM spectrum exhibits relatively gentle peak-and-trough structures, with broad peaks and shallow troughs. with overall gradual variations and a pronounced trend toward energy dispersion. At constant wind speeds, the JONSWAP spectrum generates sharper peaks, deeper troughs, steeply rising peaks, and disordered distributions. This asymmetry reflects highly concentrated energy within a narrow frequency band, most pronounced around the peak frequency. Analysis of Figures 2 (b) and (e) at identical wind speeds reveals that wave heights generated by the JONSWAP spectrum significantly exceed those of the PM spectrum. At 10 m/s wind speed, the wave heights calculated from the JONSWAP spectrum are significantly higher, validating its superiority in capturing the intense fluctuations of wind-generated waves during the growth phase. As wind speed increases from 5 m/s to 15 m/s, wave heights for both spectra rise markedly, yet the JONSWAP spectrum exhibits a greater increase. This is attributed to the amplifying effect of the peak shape parameter γ on energy peaks.

For describing fully developed waves in open ocean areas beyond the influence of the wind field, the PM spectrum is the superior choice. Its waveform exhibits a smooth transition and uniform energy distribution, making it suitable for model simulations of steady-state sea conditions. The JONSWAP spectrum is particularly well-suited for simulating developing wind waves within a finite wind field. Its narrow and steep waveform more closely approximates the dynamic behavior of underdeveloped waves in real sea conditions.

3.2 Energy Distribution Analysis of Wave Spectrum

Set the frequency analysis range to 0.02–1 Hz with a frequency resolution of 0.01 Hz. Analyze the wave spectrum energy distribution at wind speeds V of 5 m/s, 10 m/s, and 15 m/s, with gravitational acceleration $g = 9.81 \text{m/s}^2$, $\alpha = 8.10 \times 10^{-3}$, $\beta = 0.47$, The results are shown in the figure.

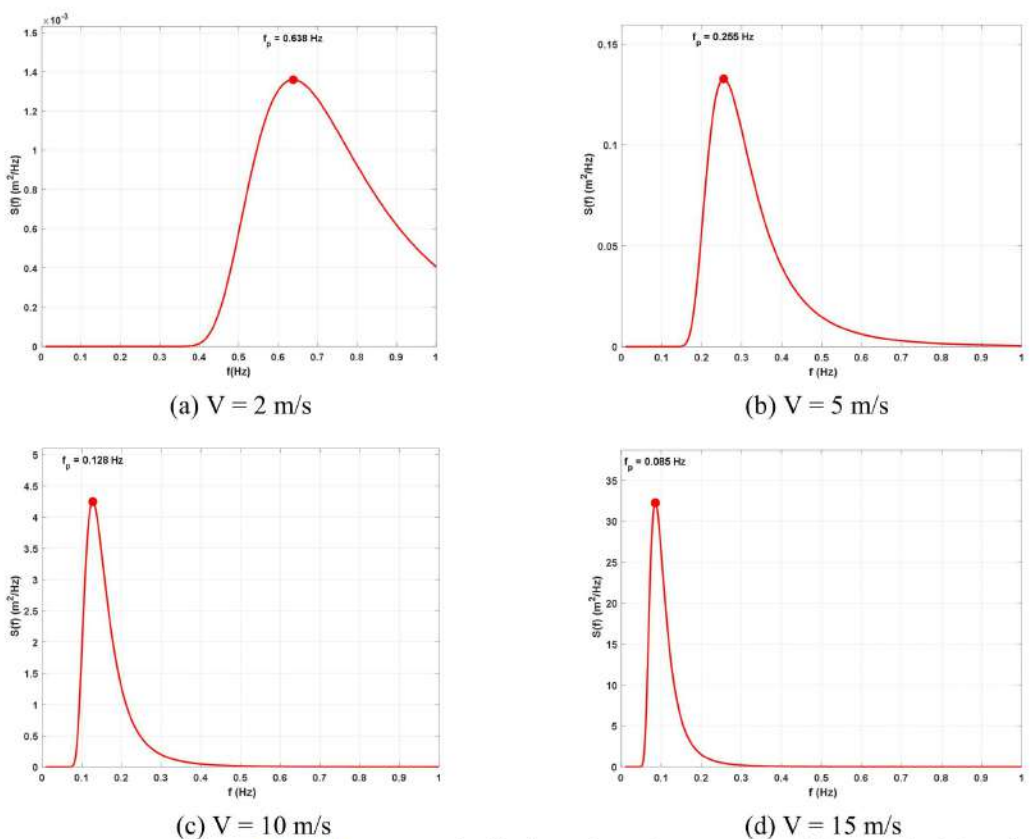


Figure 3 Energy Distribution of PM Spectrum at Different Wind Speeds

As shown in Figure 3, as wind speed increases from 2 m/s to 15 m/s, the peak frequency of the PM spectrum shifts toward lower frequencies, exhibiting a leftward shift in spectral peaks. This reflects that during high winds, the primary wave energy concentrates in the region of longer wavelengths. As wind speed increases, the spectral energy intensity rises sharply; however, the peak region becomes more dispersed without a distinct cluster of sharp peaks. This phenomenon indicates that the PM spectrum reflects a relatively uniform distribution of fully developed wave energy across the frequency band.

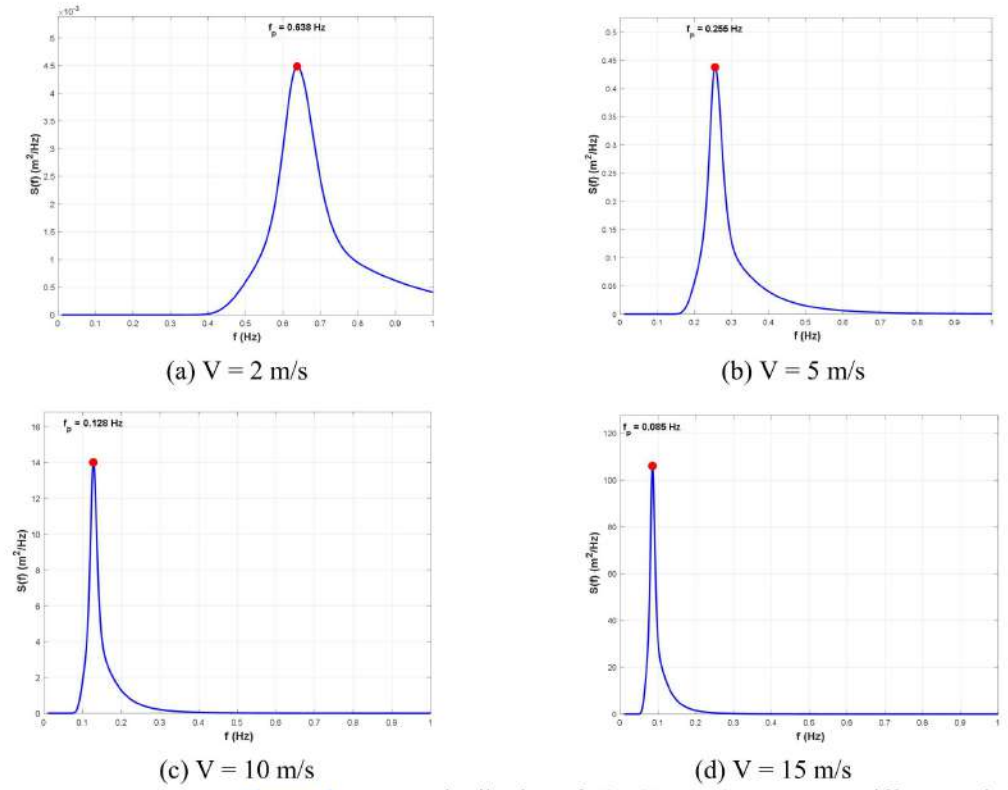


Figure 4 Energy Distribution of JONSWAP Spectrum at Different Wind Speeds

Comparing Figures 3 and 4 at the same wind speed, the energy peak of the JONSWAP spectrum is significantly larger than that of the PM spectrum. The peak spectrum shape is sharper, exhibiting stronger clustering, reflecting energy concentration within a narrower frequency band. As wind speed increases, the spectral energy level rises, and the dominant frequency also shifts toward lower frequencies, but the main peak width narrows. The peak energy amplified by the γ factor is the primary cause of the steep energy decay in the high-frequency range. The JONSWAP spectrum leverages the γ factor to amplify the spectral peaks of underdeveloped waves, providing a more accurate representation of wind-driven wave growth constrained by wind-heaving processes, thus offering high practical value.

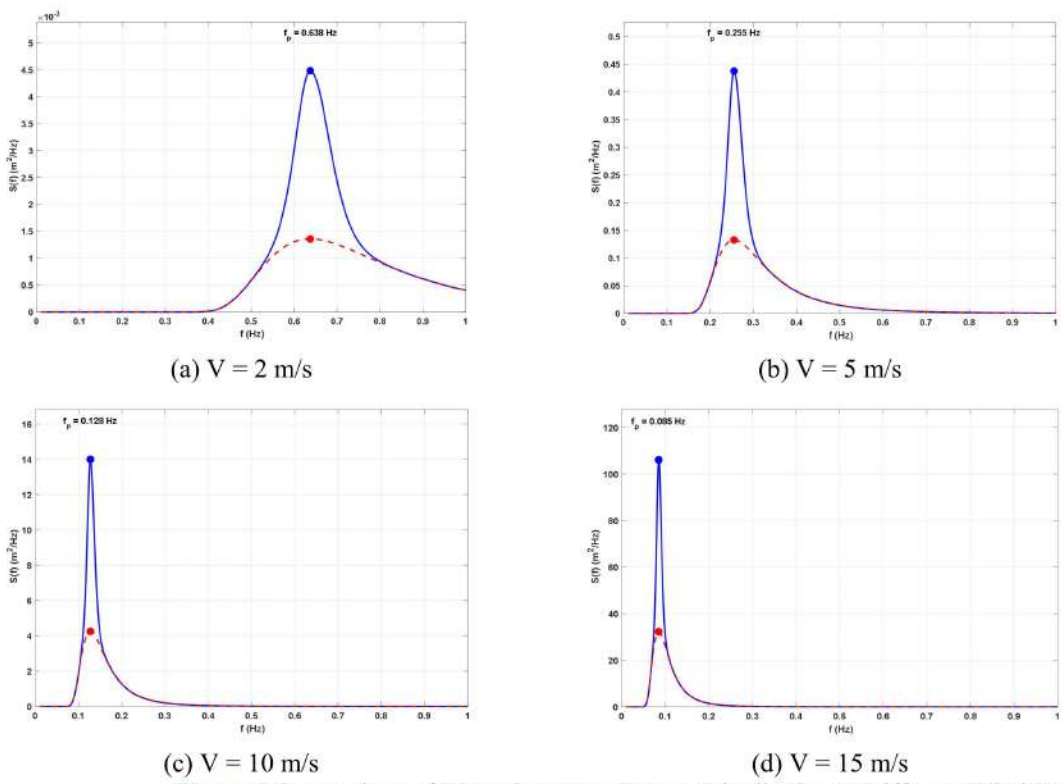


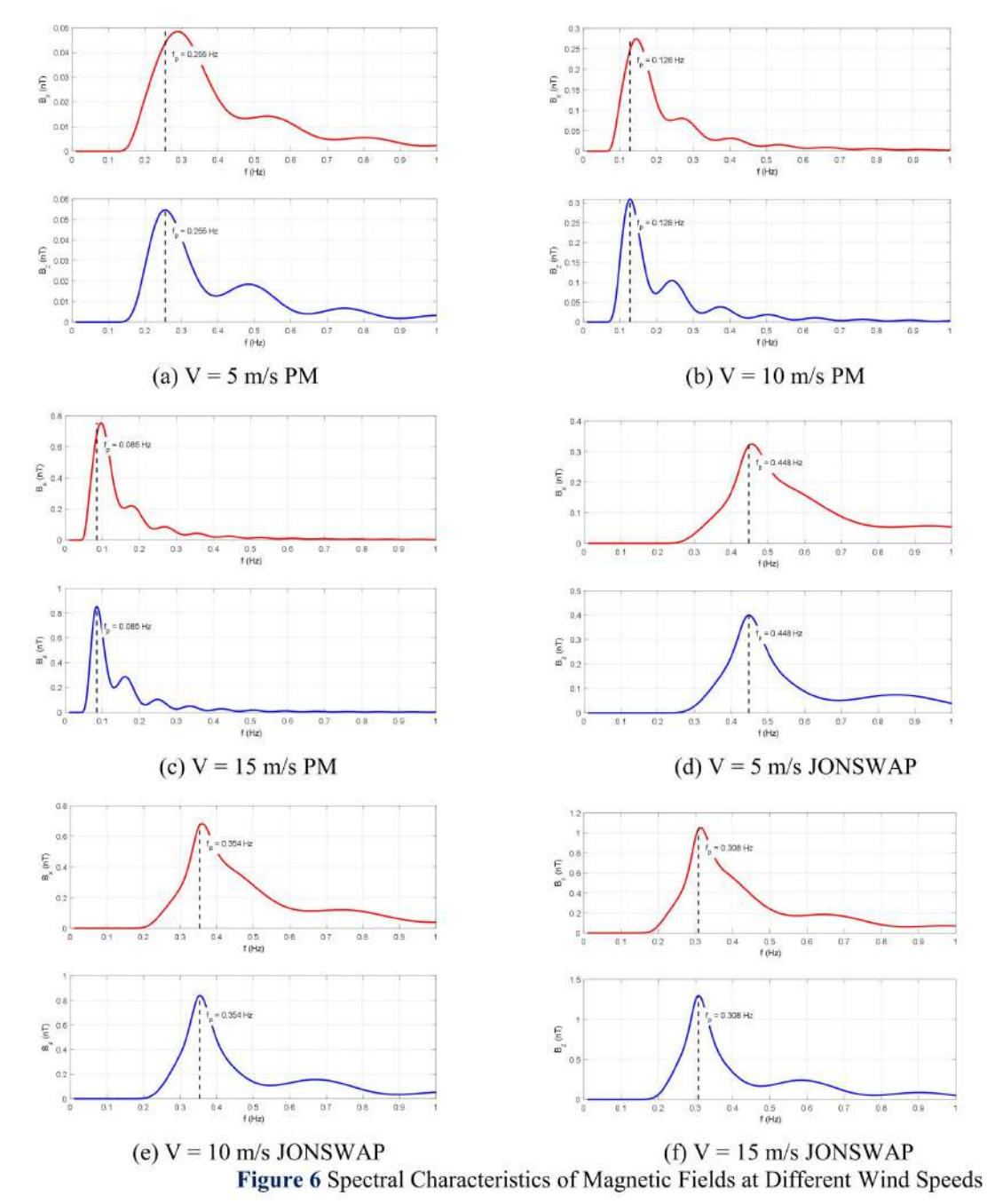
Figure 5 Comparison of Wave Spectrum Energy Distribution at Different Wind Speeds

The analysis above in Figure 5 shows that the JONSWAP spectrum exhibits sharper peak shapes. As the transition occurs toward the marginal frequency bands, the two spectral shapes gradually converge, with the JONSWAP spectrum better describing developing waves. The PM spectrum represents fully developed wave conditions. The JONSWAP spectrum amplifies the spectral peaks of immature waves through the γ factor. In practical applications, the JONSWAP spectrum aligns more closely with most real-world sea conditions. The spectral energy distribution in the non-peak frequency range shows a convergence trend, indicating similar simulation results for wave characteristics in nondominant frequency bands. Simultaneously, an increase in wind speed leads to a decrease in the spectral peak frequency.

3.3 Magnetic Field Distribution Induced by Ocean Waves

3.3.1 Spectral Characteristics of Wave-Induced Magnetic Fields

Assuming a geomagnetic field magnetic induction intensity of $B = 4.5 \times 10^{-5} \text{ T}$ $\lambda = 0.3 \text{ m}$, analyze the spectral characteristics of the wave-induced magnetic field for wind speeds of 5 m/s, 10 m/s, and 15 m/s. The results are shown in Figure 6.



Analysis of Figure 6 reveals a pronounced narrowband trend in the induced magnetic field spectra of both wave spectra,

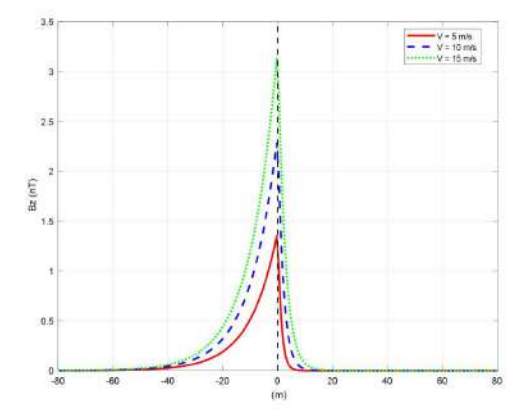
with energy distribution exhibiting significant frequency-domain clustering. Analysis of Figures 6 (a), (b), and (c)

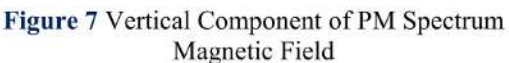
indicates that the magnetic field spectrum curve of the PM spectrum exhibits no pronounced steep changes, with a notably broad characteristic frequency band and distinct energy distribution dispersion. Analysis of Figures 6 (d), (e), and (f) reveals that the magnetic field spectrum curve of the JONSWAP spectrum demonstrates higher sharpness and more pronounced peaks, with energy primarily concentrated within specific frequency bands. The amplitude variation of the induced magnetic field positively correlates with increasing wind speed. Both spectrum types exhibit low-frequency drift in peak frequency values, manifesting as a pronounced leftward shift of spectral peaks. At a wind speed of 10 m/s, 0.354 Hz represents the approximate peak frequency for the PM spectrum; while at 15 m/s, the peak frequency decreases to approximately 0.308 Hz. Analysis under strong wind conditions reveals that wave energy significantly concentrates in the low-frequency long-wave region, causing a synchronous reduction in the dominant frequency of the induced magnetic field.

Results in Figures 6 (b) and (e) indicate that at identical wind speeds, the JONSWAP spectrum demonstrates superior performance for induced magnetic fields, particularly in the peak frequency region. At 10 m/s wind speed, the magnetic field peak of the JONSWAP spectrum increases by 1.5 to 2 times compared to the PM spectrum. This phenomenon aligns with the JONSWAP spectrum's higher energy concentration characteristic. Below the dominant frequency range, the induced magnetic field strength increases positively with frequency. In the spectral range to the right of the dominant frequency, the induced magnetic field exhibits a decaying characteristic as frequency increases. Its distribution pattern closely resembles the wave energy spectrum, confirming that the induced magnetic field spectrum is directly regulated by the wave energy distribution.

In summary, the wave-induced magnetic field spectrum exhibits pronounced narrowband concentration, with its dominant frequency aligning with the peak frequency of wave energy. The spectral characteristics of the induced magnetic field are highly dependent on wind speed. with both the shift of the dominant frequency toward lower frequencies and the enhancement of magnetic field amplitude closely related to increased wind speed. Compared to the PM spectrum, the JONSWAP spectrum generates stronger and more concentrated induced magnetic fields at the same wind speed, making it more suitable for describing developing wind waves and their electromagnetic noise background. 3.3.2 Characteristics of Wave-Induced Magnetic Field Component Distribution

Using the Weaver electromagnetic theory model, the following geomagnetic parameters were set: magnetic induction intensity $B = 4.5 \times 10^{-5} \, \text{T}$, magnetic inclination angle $I = 60^{\circ}$, and wave propagation direction forming a 30° angle with the geomagnetic north pole. At time t=0, with frequency segmentation parameters M=N=50 (frequency range 0.02–1 Hz), the distribution of the vertical component Bz of the induced magnetic field along depth was calculated, with results shown in the figure.





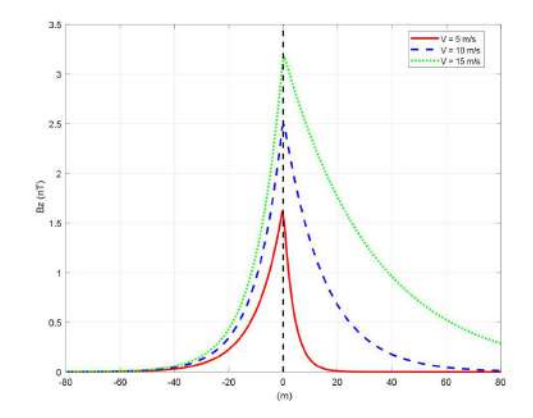
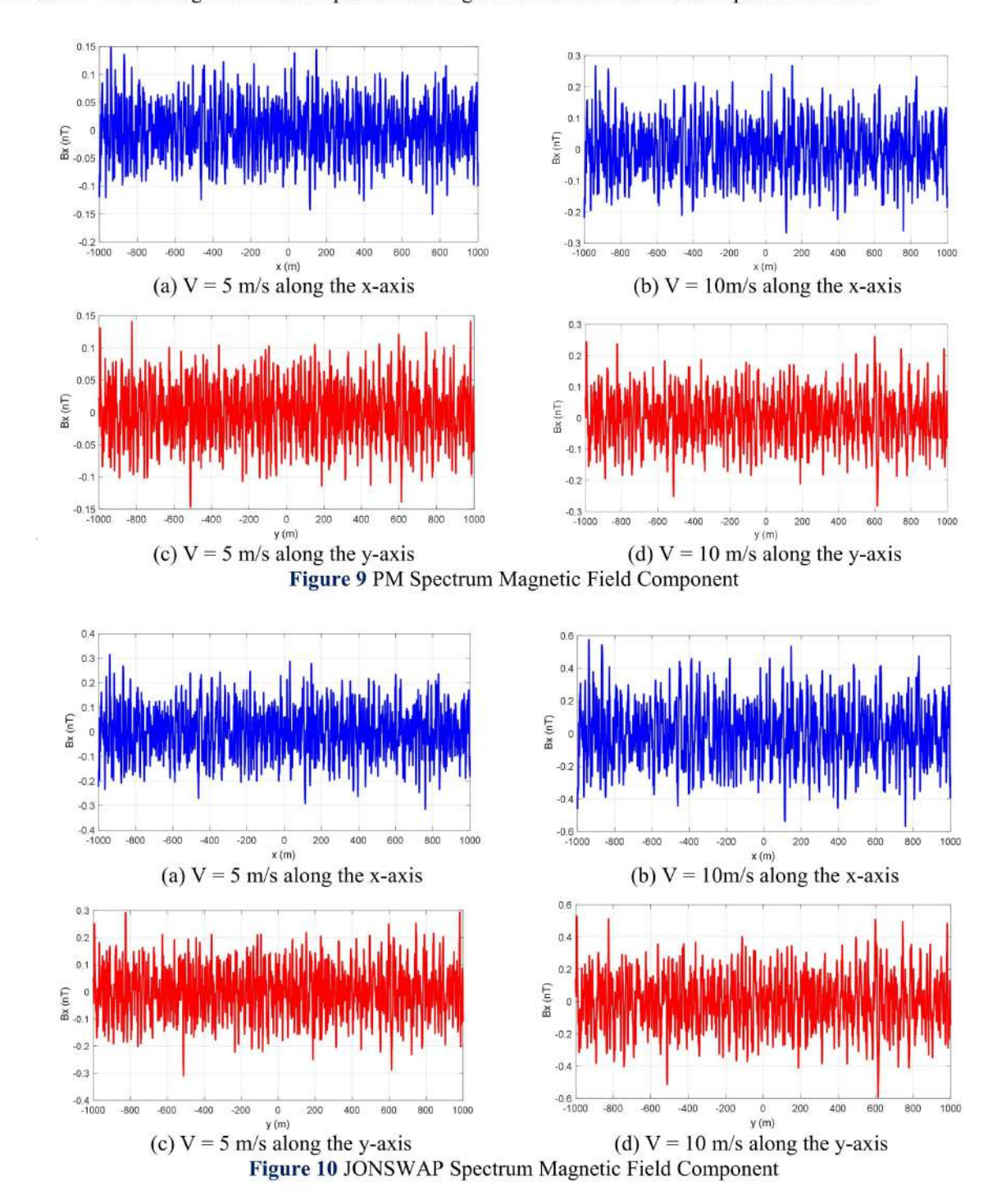


Figure 8 Vertical Component of JONSWAP Spectrum Magnetic Field

As shown in Figure 7, the spatial distribution of the vertical magnetic field component in the PM spectrum is relatively gentle, with sparse and uniformly varying contour lines. The peak magnetic field regions exhibit extensive distribution characteristics, consistent with the energy equilibrium features of mature waves as characterized by the PM spectrum. As seen in Figure 8, the spatial fluctuations of the vertical magnetic field component in the JONSWAP spectrum are more pronounced and structurally more complex, presenting multiple distinct clusters of extreme values. The magnetic field intensity gradient markedly increases, revealing the energy-dense and steep-wave characteristics of growing-stage waves simulated by the JONSWAP spectrum. Under identical wind speed conditions, the peak value of the Bz component in the JONSWAP spectrum exceeds that of the PM spectrum, a phenomenon directly related to the stronger wave energy peaks in the JONSWAP spectrum.

The vertical magnetic field distributions in Figures 7 and 8 both form periodic stripe structures correlated with wave direction. Regarding the JONSWAP spectrum's magnetic field distribution, this periodic pattern exhibits more pronounced fragmentation and localized clustering, reflecting the irregularity of the wave growth stage. The spatial characteristics of the vertical magnetic field component are directly influenced by the coupling between waveform and geomagnetic field. The JONSWAP spectrum exhibits increased peak sharpness and pronounced trough depression,

leading to greater variations in the speed and extent of seawater cutting through geomagnetic field lines. Consequently, the induced vertical magnetic field component is stronger and exhibits more intense spatial variations.



Comparing Figures 9 and 10 reveals that for the horizontal component of the PM spectrum magnetic field, the Bx amplitude ranges approximately from ± 0.15 nT at a wind speed of 5 m/s to ± 0.3 nT at 10 m/s. The amplitude variation remains relatively stable with minimal fluctuation. For the JONSWAP spectrum's horizontal magnetic field component, the Bx amplitude ranges from approximately ± 0.3 nT at 5 m/s wind speed to ± 0.6 nT at 10 m/s wind speed. At the same wind speed, the amplitude of the JONSWAP spectrum's horizontal magnetic field component is approximately twice that of the PM spectrum. Both spectra exhibit distinct periodic oscillations along the x-direction propagation axis, with oscillation periods directly correlated to wave wavelengths. The JONSWAP spectrum shows more pronounced oscillations and more prominent local extrema. Along the y-direction, the PM spectrum exhibits relatively smooth variations with largely stable amplitude, while the JONSWAP spectrum also displays significant oscillatory characteristics. Due to the wind direction being set at $\pi/4$, Bx exhibits similar propagation characteristics in both the x and y directions. As wind speed increases from 5 m/s to 10 m/s, the horizontal magnetic field component amplitudes of both spectra nearly double, maintaining consistent distribution patterns while exhibiting significantly amplified fluctuations. This reflects the positive correlation between wind speed and induced magnetic field strength.

In summary, under identical wind speeds, the horizontal magnetic field component amplitude generated by the JONSWAP spectrum is significantly greater than that of the PM spectrum, typically reaching approximately twice the PM spectrum's value. The PM spectrum exhibits relatively uniform horizontal component distribution with gentle fluctuations, making it suitable for describing fully developed sea conditions. In contrast, the JONSWAP spectrum features intense horizontal component fluctuations with pronounced local characteristics, more accurately reflecting the nonlinear properties of developing wind-driven waves. With the wind direction set to $\pi/4$, the horizontal magnetic field components display similar distribution patterns in both the x and y directions. However, the JONSWAP spectrum exhibits more pronounced fluctuations in the y direction.

4 CONCLUSION

This paper employs the Pierson-Moskowitz wave spectrum, JONSWAP spectrum, and Weaver electromagnetic theory to simulate two-dimensional random sea surfaces under wind speeds of 5 m/s, 10 m/s, and 15 m/s using the Monte Carlo method. It analyzes the distribution of wave-induced magnetic fields through Maxwell's equations, The system analyzes the sea surface morphology, wave spectrum energy, and spatial/spectral characteristics of the induced magnetic field, leading to the following conclusions:

- (1) The PM spectrum generates waves with gentle undulations, broad crests, shallow troughs, and uniformly distributed energy, effectively reflecting fully developed wave characteristics. The JONSWAP spectrum produces waves with sharper crests, deeper troughs, and increased asymmetry, exhibiting narrow-band energy concentration that better aligns with actual wave development patterns under finite wind conditions.
- (2) Comparing the energy distribution characteristics reveals: under identical wind speeds, the peak energy of the JONSWAP spectrum significantly exceeds that of the PM spectrum, with a more concentrated peak distribution and stronger energy clustering. During wind acceleration phases, both spectra exhibit low-frequency shifts in peak frequency. The JONSWAP spectrum achieves incremental peak energy through its γ factor, enabling more effective characterization of wave energy during the growth phase.
- (3) Wave-induced magnetic field spectra generally exhibit narrowband clustering phenomena: both wave spectra induce magnetic fields with typical narrowband spectra, where the dominant frequency shifts toward lower frequencies as wind speed increases. The amplitude of the JONSWAP spectrum-induced magnetic field at its peak frequency is approximately 1.5–2 times that of the PM spectrum, further corroborating its energy-focusing characteristic. In the low-frequency band, magnetic field strength increases with frequency, while the field begins to weaken upon reaching the high-frequency band.
- (4) Significant spatial distribution differences among induced magnetic field components: At comparable wind speeds, both the vertical and horizontal components of the JONSWAP spectrum-induced magnetic field exhibit significantly higher amplitudes than the PM spectrum, with the horizontal component reaching twice the amplitude of the PM spectrum. The spatial distribution of JONSWAP spectrum magnetic field components shows more pronounced fluctuations, reflecting the non-uniform characteristics of developing wind waves.

COMPETING INTERESTS

The authors have no relevant financial or non-financial interests to disclose.

REFERENCES

- [1] Pierson W J, Moskowitz L. A Proposed Spectral Form for Fully Developed Wind Seas Based on the Similarity Theory of S. A. Kitaigorodskii. Journal of Geophysical Research Atmospheres, 1963, 69(24):5181-5190.
- [2] Weaver J T. Magnetic variations associated with ocean waves and swell. Journal of Geophysical Research, 1965, 70(8):1921-1929.
- [3] Pedersen T, Lilley T, Hitchman A. Magnetic signals generated by ocean swells. Aseg Extended Abstracts, 2003, 2003:1-4.
- [4] TANG Jinfei, GONG Shenguang, WANG Jingen. Calculation of the energy distribution of the wave-induced magnetic field based on the Neumann spectrum and the PM spectrum. Journal of Naval University of Engineering, 2001, 13(4): 82-86.
- [5] ZHANG Zili, WEI Wenbo, LIU Baohua. Theoretical calculation of electromagnetic field induced by sea waves. Acta Oceanologica Sinica, 2008, 30(1): 42-46.
- [6] Zhu X, Xia M. Magnetic Field Induced by Wake of Moving Body in Wind Waves. Progress In Electromagnetics Research, 2014, 149:109-118.
- [7] Wang Wei. Simulation and Electromagnetic Calculation of Wake Trails from Surface Vessels. Xi'an University of Electronic Science and Technology, 2015.
- [8] Zhang Baoqiang. Research on Suppression Methods for Electromagnetic Noise Induced by Ocean Waves Based on Wavelet Analysis of Marine Mt Data. Ocean University of China, 2018.
- [9] LIN Zhiheng, LI Yuguo. Numerical calculation method of induced magnetic field by seawater motion. Journal of Ocean University of China (Natural Science Edition), 2019, 49(2): 74-78.
- [10] ZHOU Chun, LI Yuguo, ZHANG Baoqiang. Numerical simulation and characteristic analysis of electromagnetic field induced by variable velocity seawater motion. Oceanologia et Limnologia Sinica, 2019, 50(2): 261-268.

- [11] Zhang Jiansheng. Research and Measurement of Optical Characteristics of Wake Flow. Xi'an: Xi'an Institute of Optics and Precision Mechanics, Chinese Academy of Sciences, 2001.
- [12] Zhang Chengji. Simulation of Ship Wakes and Characteristics of Induced Magnetic Field Distribution. Xi'an University of Technology, 2018.
- [13] Xiao Chen. Electromagnetic Characteristics of Bubble Curtains in Ship Wakes. Xi'an University of Technology, 2016.
- [14] YAN Linbo, ZHANG Jiansheng, DONG Min, et al. Characteristic Analysis and Simulation System Design of Multi-Ship Wake Magnetic Anomaly. Journal of Unmanned Undersea Systems, 2024, 32(5): 801-807.
- [15] LAN Qing, YAN Linbo, REN Binbin. Simulation Analysis of Induced Electromagnetic Field in KCS Ship Wake. Journal of Unmanned Undersea Systems, 2024, 32(5): 818-822+832.
- [16] Ye Anle, Li Fengqi. Physical Oceanography . Qingdao: Ocean University of China Press, 1990.
- [17] MUNK W H. Directional recording of swell from distant storms. Phil Trans Roy Soc London, 1962, 254: 565-584.